Scientific African 15 (2022) e01107

Contents lists available at ScienceDirect

Scientific African

journal homepage: www.elsevier.com/locate/sciaf

Exploring the inhibitory mechanism of resorcinylic isoxazole amine NVP-AUY922 towards the discovery of potential heat shock protein 90 (Hsp90) inhibitors

Ayanda M. Magwenyane[a], Monsurat M. Lawal[a,*], Daniel G. Amoako[a,b], Anou M. Somboro[a,b], Clement Agoni[a], Rene B. Khan[a], NdumisoN. Mhlongo[a], Hezekiel M. Kumalo[a,*]

[a] Drug Research and Innovation Unit, Discipline of Medical Biochemistry, School of Laboratory Medicine and Medical Science, University of KwaZulu-Natal, Durban 4000, South Africa
[b] Biomedical Resource Unit, College of Health Sciences, University of KwaZulu-Natal, Durban 4000, South Africa

ARTICLE INFO

Article history:
Received 9 August 2021
Revised 28 December 2021
Accepted 25 January 2022

Editor: DR B Gyampoh

Keywords:
Pharmacophore-based virtual screening
Molecular docking
Molecular dynamics
ONIOM method
Hsp90 N-terminal
NVP-AUY922

ABSTRACT

Heat shock protein 90 (Hsp90) is an ATP-dependant molecular chaperone that facilitates protein maturation while protecting cancer cells from temperature-induced stress. Hsp90, therefore, remains an attractive target for anticancer drug development. The study aimed to use multidimensional computational drug design to discover new hit compounds that potentially interact with the ATP pocket of Hsp90 and can be used as effective anticancer drugs. An in-house pharmacophore-based virtual screening (PBVS) protocol was used to identify potential Hsp90 inhibitors. Molecular docking, screening, and molecular dynamics simulations (MD) are the models that were used to refine the selection. Based on the structural features of the resorcinol-isoxazole amine NVP-AUY922 (NVP) with significant binding affinity to Hsp90, PBVS enabled the identification of 77 compounds, 10 of which showed favourable binding energy over NVP. Amongst the ten selected compounds, ZINC20411962, ZINC13120102, and ZINC15905860 showed the most favoured interaction with the N-terminus of Hsp90. The root-mean-square deviation (RMSD), root mean square fluctuation (RMSF) and gyration radius (RoG) analyses from the MD simulations confirmed that the three identified compounds are stable at the ATP-binding site of the N-terminus of Hsp90. The MD parameters studied also showed that ZINC20411962 formed the most stable complex with the protein, which was confirmed by the ONIOM calculation with the most negative entropy value of –28 kcal/mol and a binding free energy value of –63 kcal/mol. The compounds interacted with the catalytic residues Thr184, Phe138, Met98 Gly97, and Asn106, which are crucial for the inhibition of Hsp90. The compound ZINC20411962 also has appreciable physicochemical, medicinal, pharmacokinetics, and drug-like properties that could uniquely position it as a potential lead for Hsp90 inhibition. The applied methodology herein represents a promising approach that could pave

* Corresponding authors.
E-mail addresses: lawalmonsurat635@gmail.com (M.M. Lawal), KumaloH@ukzn.ac.za (H.M. Kumalo).

https://doi.org/10.1016/j.sciaf.2022.e01107

way for the successful identification of compounds inhibiting crucial targets in diseases, including terminal ones, like cancer.

Introduction

The importance of heat shock protein 90 (Hsp90) in all branches of eukaryotes and bacteria has attracted the attention of researchers because it helps numerous proteins fold and mature in normal and cancer cells [1]. Hsp90 protects cells under stress conditions [2] and accounts for 1,2% of total protein in unstressed cells, while it increases to 4–6% of cellular proteins when heated [3]. When comparing tumour cells and normal cells, Hsp90 was found to be constitutively expressed at 2–10 fold higher levels in tumour cells [4]. This overexpression suggests that this protein is required for tumour cell growth and survival. Therefore, Hsp90 is a target for anti-cancer drug development [5].

Some Hsp90-dependant proteins involved in cancer are anaplastic lymphoma kinase (ALK), v-raf murine sarcoma viral oncogene homologue B1 (BRAF), epidermal growth factor receptor (EGFR), ErbB family 2 (ERBB2), and insulin-like growth factor-1 receptor (IGF1R). V-kit Hardy-Zeckerman 4 feline sarcoma viral oncogene homologue (KIT) and Met-proto-oncogene are also Hsp90-dependant and have been linked to cancer [5,6]. The EML4-ALK fusion protein and four other ALK fusion proteins are involved in the development of approximately 5% of non-small cell lung carcinomas [7]. Overexpression of EGFR is associated with poor clinical outcomes in a variety of cancers, including head and neck, larynx, oesophagus, stomach, pancreas, colon, kidney cells, bladder, breast, ovarian, cervical, prostate, non-small cell lung cancer, papillary thyroid cancer, melanoma and glioma [8].

The expression of Hsp90 is a signature of several cancers, including cervical, colon, liver, brain, kidney, lung, breast, and prostate cancers [9,10]. In a recent review, Birbo et al. [9] summarized the role of Hsp90 in cancer, its secretion enhances the aggression of the tumour cells in the early phase metastasis. Increased invasiveness happens from Hsp90α secretion via exosomes from aggressive cancer cells, it greatly enhances malignancy. The mitochondrial Hsp90, otherwise called TRAP1, is available within the cell [10]. TRAP1 is implicated in tumorigenesis, and its inhibition stimulates sudden inactivation of membrane potential, resulting in membrane rupture and apoptosis initiation [10]. Therefore, the development of potent Hsp90 inhibitors with high selectivity and specificity is of great importance.

Radicicol (RD) and geldanamycin (GA) have been identified as natural Hsp90 inhibitors that bind directly to the ATP pocket in the N-terminal domain and compete with ATP [11]. n cancer cells, Hsp90 has a high affinity for ATP and inhibitors, whereas in normal cells Hsp90 is in a non-complexed state [12]. The binding affinity of 7-AAG (an analogue of a natural inhibitor) and Hsp90 from tumour cells is reported to be 100-fold higher than that of Hsp90 from normal cells [13]. Inhibition of Hsp90 can stop the function of all the above-mentioned client proteins, resulting in potent, selective anti-cancer activity [14]. Researchers have developed several Hsp90 inhibitors, including ansamycin-purine and resorcinol derivatives, but none of them made it to regulatory approval. The potent molecules showed limited clinical activity as single agents, off-target and Hsp-related toxicities, such as ocular disease [15,16].

The design of new Hsp90 inhibitors enables the identification of potent hit compounds for which computer-aided drug design (CADD) has found application. CADD is quite attractive in drug discovery projects due to its cost-effectiveness in obtaining potentially active compounds with a higher probability of success promptly. Saxena et al. [17] used CADD methods, including virtual screening and quantitative structure-activity relationship (QSAR), to identify and model Hsp90 inhibitors. Using 103 Hsp90 inhibitors, they [17] used catalyst software to create a pharmacophore model using the software GOLD for ligand docking to Hsp90. In another study [2] by the same research group [17], they identified the key chemical features of Hsp90 inhibitor activity by creating a 3D-QSAR pharmacophore model with a series of 2-amino-6-halopurine, 70 substituted benzothiazolothio purines, and pyridinothiazoltio purines. The 3D-QSAR pharmacophore model resulted in the selection of 5 hit structures docked to Hsp90 amongst the identified compounds from the Maybridge and National Cancer Institute (NCI) 2 databases [2].

Also, Sanam et al. [18] used a pharmacophore model to select 455 compounds from a library of 1 million compounds. After molecular docking to Hsp90 and a cytotoxicity assay, five of these 455 compounds showed IC_{50} values of less than 50 µmol. Sakkiah et al. [19] used pharmacophore-based virtual screening (PBVS) and molecular docking to obtain four compounds with potential Hsp90 inhibition. In another study, they [19] identified 36 compounds as Hsp90 inhibitors using 3D-QSAR PBVS and molecular docking [20]. Huang et al. [21] downloaded 9050 compounds from InterBioScreen Ltd's natural product using four scoring functions in the GOLD software suite with protein nuclear magnetic resonance (NMR) spectroscopy. Of the four compounds found, two interact strongly with Hsp90 with binding constants of less than 5 µmol. The present research reports thus support the relevance of CADD by virtual screening as an important tool for identifying hit compounds with potential interaction with a specific target.

Amongst the synthetic Hsp90 inhibitors, we select NVP-AUY922 (NVP), which has already been tested in phase I and II clinical trials [22]. The novel Hsp90 inhibitor, which is not a geldanamycin, is stable in the ATP pocket [23]. Previously, Liu

et al. [24] investigated the effect of NVP on the survival of PTC cell lines KI and IHH4. They observed that treatment of these cell lines with NVP caused cleavage of PARP and caspase-3 proteins and altered the expression of surviving, a client protein of Hsp90. They concluded that NVP induces apoptotic cell death in PTC. They concluded that NVP induces apoptotic cell death in PTC cells. We [23] recently applied a molecular dynamics approach to RD and NVP as potent Hsp90 inhibitors and found that NVP is more stable in the ATP pocket and has a better interaction than RD. The study [23] motivated the present investigation to identify potent Hsp90 inhibitors based on the properties obtained upon inhibition of NVP. Therefore, this study aims to discover new hit compounds with potential interaction with the ATP pocket of Hsp90 as potent anticancer drugs using computational drug design.

There are indeed existing studies on computational approaches, including pharmacophore modelling, towards identifying molecules of interest targeting Hsp90. However, the integrated methods herein are unique to our research, especially, the per-residue-based pharmacophore modelling method that scans the crucial moieties driving the inhibitor-enzyme interaction as a query for virtual screening. Our study is amongst the few that screens conventional compounds from the ZINC database using an ongoing clinical trial molecule as the parent material. We also probe beyond the popular MD simulation method to quantify the affinity of the identified compounds towards NT Hsp90 with a hybrid quantum mechanics/molecular mechanics (QM/MM) method. This model enabled improved estimation of the potent molecules' interaction with NT Hsp90 at near experiment accuracy.

Materials and methods

System preparation

The x-ray crystal structure of Hsp90 in complex with ATP (PDB code: 3T0Z [25]) is available in the Protein Data Bank. We added missing residues to the retrieved 3T0Z using the graphical user interface of Chimera [26] molecular modelling tool. Alterations and visualization of ligands entail using Chimera and Avogadro visualization software.

Molecular docking

We used AutoDock Vina [27] software for docking calculations, assign Gasteiger partial charges to the ligands, and obtain docked information using the Lamarckian genetic algorithm [28]. The size of the grid box was $x = 36$ Å, $y = 36$ Å, $z = 26$ Å, and $x = -10.000$ Å, $y = 2.528$ Å and $z = -15.417$ Å for the dimensions encapsulating the active site residues Asn51, Ala55, Lys58, Ans83, Asp86, Ile96, Gly97, Met98, Asn106, Leu107, Lys112, Phe138, Ile151, Tyr160, Ala161, Asp165, Glu178, Met180, Thr184, Lys185, Ile187. We reported the observed binding scores and interactions for the ten compounds with higher binding energies than NVP. We did not consider protein flexibility because the procedure is for compound coupling to the catalytic active site as the target region. The data outcome will probably be different if we incorporate protein flexibility during the docking and such procedure might find non-active site as plausible binding regions, which is beyond the scope of the present research.

MD simulations

We apply MD simulation at 50 ns to provide insight into the binding mechanism of ligand on Hsp90 using the GPU version PMEMD algorithm incorporated in AMBER14 for unrestrained production in explicit solvent. With the LEAP module of AMBER14, we add missing hydrogens and counter ions for neutralisation. All the systems were then solvated using an orthorhombic box of TIP3P water molecules at 10 Å from all the protein atoms with specific periodic boundary conditions. We use the particle mesh Ewald method with a direct space and Van der Waals cut-off at 12 Å to calculate long-range electronic interactions. The procedures for the pre-MD production run, which are in three steps, minimisation, heating, and equilibration), have been described in the literature [23]. Further analysis of the saved trajectories entails using the AMBER14 tools, PTRAJ, and CPPTRAJ modules to extrapolate the RoG, RMSD, and RMSF.

Per-residue energy decomposition (PRED) pharmacophore model

A pharmacophore model was created by exploring the structural and chemical features of the protein and the ligand. We calculate PRED using molecular mechanics Poisson–Boltzmann surface area (MMPBSA) [29,30] after running 50 ns MD simulations of the hit compound-Hsp90 complex to create a PRED-based pharmacophore model. This approach enabled estimation of the individual crucial residue total energy contribution to the binding free energy using Eq. (1). Energetics of ligand-residue interactions ($\Delta G_{\text{inhibitor–residue}}$) incorporates the energy terms: electrostatic contribution (ΔE_{ele}), van der Waals contribution (ΔE_{vdW}), polar contribution (ΔG_{pol}), and non-polar contribution (ΔG_{nonpol}).

$$\Delta G_{inhibitor-residue} = \Delta E_{vdW} + \Delta E_{ele} + \Delta G_{pol} + \Delta G_{nonpolar} \quad (1)$$

The crucial residues that are part of the active site and interact with the ligand are Leu48, Ser52, Asp54, Ala55, Lys58, Asp93, Ile96, Asp102, Asn106, Leu107, Lys112, Phe138, Val150, Hip154, Thr184. We use the ZINC Pharmer interface to retrieve the pharmacophore model using the default characteristics, including hydrogen bond donor (D), aromatic (R), hydrogen bond

acceptor (A), positive ion (P), negative ion (N), and hydrophobic (H). Furthermore, the PRED-pharmacophore model was used to screen the ZINC database for compounds with similar characteristics to obtain novel hits.

Thermochemistry calculation

The coordinates of the simulated complexes were extracted and prepared for Our Own N-layered Integrated molecular Orbital and Molecular Mechanics (ONIOM) calculation. A two-layered ONIOM hybrid QM/MM model was employed to analyse the binding affinity of the identified potentially active Hsp90 inhibitors. ONIOM approach offers a unique way of partitioning the protein/molecule into reactive and less reactive parts. Usually, investigators use a higher level of theory, such as density functional theory (DFT) for the reactive residues and the ligand, and a lower level such as MM force field for the remaining system. The approach allows an improved molecular properties estimation compared to the default MM model in MD simulation.

In this calculation, we put nine prominent residues (Asn51, Ala55, Ile96, Met98, Asn106, Leu107, Val136, Phe138, Thr184) marked crucial through the PRED analysis and ligands to a high (DFT) level using B3LYP and 6–31+G(d) combination and AMBER MM force field for the remaining enzyme structure. Some related investigations have shown that the selected ONIOM theoretical level is sufficient for enzyme-ligand binding energy calculation. The applied two-layered ONIOM (ONIOM2) calculation allows the estimation of the binding free energies and other thermodynamic parameters of the potent Hsp90 inhibitors complexes. The ONIOM calculation involves geometry optimisation of the ligands, enzyme, and enzyme-ligand complexes using B3LYP/6–31+G(d):AMBER and frequency calculation to obtain the thermochemistry.

Eq. (2) describes the total interaction energy attained from the ONIOM2 calculations, where ΔE_{model} is the energies of the model system calculated at both high and low levels, and ΔE_{real} represents the energy of the entire (exact) system.

$$\Delta E_{ONIOM} = \Delta E_{model,\ high} + \Delta E_{real,\ low} - \Delta E_{model,\ low} \tag{2}$$

The relative binding free energy change (ΔG_{bind}) of all the complexes was derived from the frequency calculations as shown in Eq. (3).

$$\Delta G_{ONIOM} \approx \Delta G_{bind} = G_{complex} - G_{protein} - G_{ligand} \tag{3}$$

The thermodynamics quantities (enthalpy and entropy) changes were also obtained from the ONIOM calculations like the ΔG estimation.

ADME properties prediction

Drug design and identification are beyond interaction mode and affinity for the targets [31]. Other properties obtainable using *in silico* tools are pharmacokinetics, physicochemical, drug-like, and medicinal potentials of potent molecules which are crucial to drug design. Determining these parameters often serve as ADME – absorption, distribution, metabolism, excretion prediction. We used SwissADME [32] to predict the ADME components of the identified potent molecules with the functional groups driving their binding potentials as plausible Hsp90 inhibitors.

Results and discussion

Binding site characteristics analysis

The design of new hit compounds requires an analysis of the binding site characteristics and binding mechanism of inhibitors at the ATP-binding site of the N-domain of Hsp90. Fig. 1 shows various features of the ATP binding site residues as predicted in the Discovery Studio visualisation software. The ATP pocket has both hydrophobic and hydrophilic sites [33]. Due to the presence of acidic residues, this region is negatively charged. Therefore, the hydrogen bonding donor groups in ligands can interact with this region to enhance the binding of ligands to the ATP pocket of the N-domain of Hsp90. The hydrophobic residues interact with the ligands via van der Waals (vdW) interactions.

Pharmacophore-based virtual screening (PBVS)

NVP (Fig. S1) is an N-domain inhibitor of Hsp90 with an IC_{50} value of 13 nM for Hsp90α and 21 nM for Hsp90β in cell-free assays, reportedly tested in phase I/ II clinical trials [34,35]. The alignment of NVP in the ATP pocket served as an orientation for PBVS, resulting in a pharmacophore. We use the created pharmacophore to search a chemical database of 3D structural compounds, which yielded 150 hits. We dock these 150 hits to the active site of the crystal structure (PDB code: 3T0Z) using AutoDock Vina to assess their chemical and physical feasibility. Of the 150 hits, about 77 compounds proved plausible for binding to the active site. Table 1 shows the top ten hits with higher binding affinity than NVP, where the value for NVP is –7.7 kcal/mol.

Amongst the compounds obtained, ZINC43130413 is a known Hsp90 inhibitor (ganetespib) that has been tested in clinical trials [34] and is currently being tested in human trials [36]. Therefore, the hit compounds obtained by the virtual screening method are potential Hsp90 inhibitors. Further refinement using Lipinski's rule of five, based on the number of hydrogen

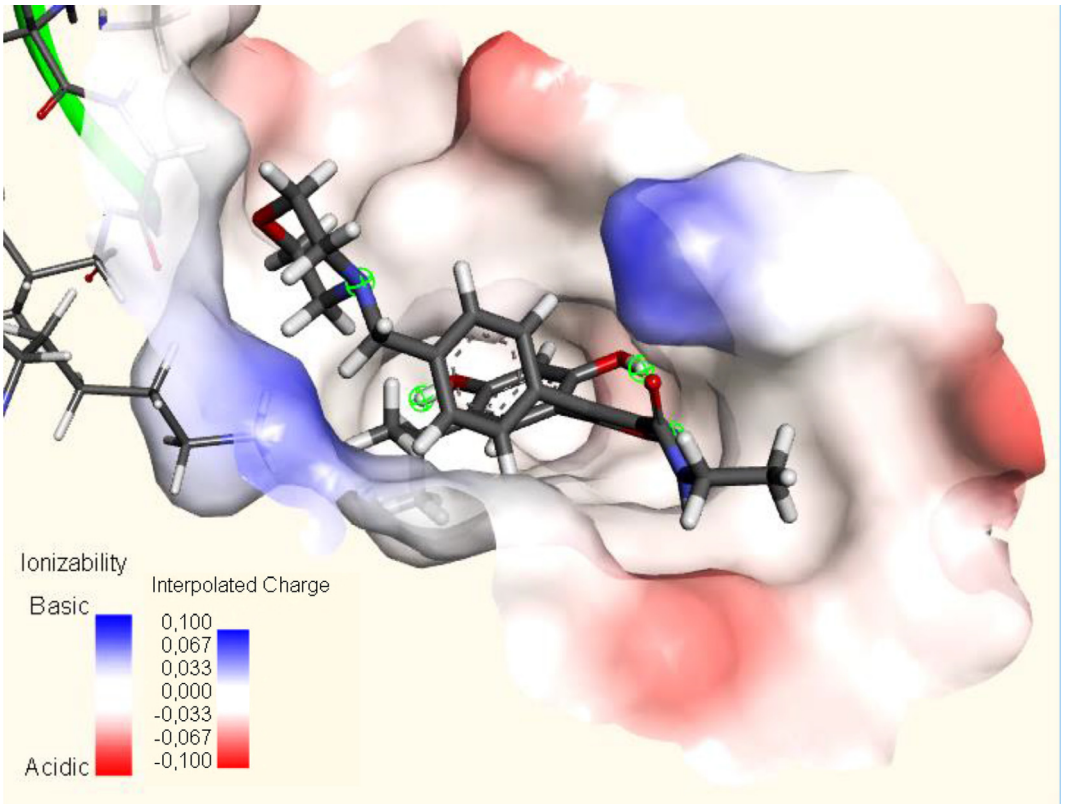

Fig. 1. Characteristics of ATP-binding site; acidity (red), basicity (blue), and interpolated charges (red = more negative, and blue = more positive).

Table 1
ZINC ID, AutoDock Vina score (in kcal/mol), and physicochemical properties of the top ten compounds with binding scores greater than NVP score.

Number	ZINC ID	AutoDock Vina score	MW	cLogP	NRB	NHBD	NHBA
1	20,411,962	−8.9	393.15	0.889	8	2	8
2	13,120,102	−8.8	406.44	3.621	6	3	7
3	15,905,860	−8.7	368.35	3.144	4	3	7
4	43,130,413	−8.7	364.41	3.254	3	3	6
5	05,247,960	−8.6	396.40	3.577	4	3	7
6	5,013,091	−8.6	351.43	4.636	3	3	5
7	934,320	−8.6	405.40	5.346	3	3	5
8	407,291	−8.6	338.36	3.754	3	3	5
9	18,114,979	−8.5	348.41	3.912	3	3	5
10	4,585,991	−8.5	348.32	4.732	3	3	3

MW = molecular weight, cLogP = calculated partition coefficient, NRB = number of rotatable bonds, NHBD = number of hydrogen bond donors, NHBA = number of hydrogen bond acceptors.

bond donors and acceptors, molecular weight, and cLogP, yielded three hits. After evaluating the compounds according to Lipinski's rule, the three hits with the highest binding affinities to the active site are ZINC20411962 (−8.9 kcal/mol), ZINC13120102 (−8.8 kcal/mol), and ZINC15905860 (−8.7 kcal/mol). We use MD simulations with a duration of 50 ns to investigate the binding mechanism and stability of the best hits against the N-domain of Hsp90 and to build a model that corresponds to realistic conditions.

The binding poses and interaction of compound NVP with Hsp90

Figure S2 shows the binding position and interaction of NVP with the ATP pocket of the N-terminal Hsp90. Threonine 184 formed a hydrogen bond (HB) with an oxygen atom in the isoxazole ring at 5.22 Å and another HB with an oxygen atom in the resorcinol ring (distance: 1.92 Å). Aspartic acid 93 formed an HB with hydrogen (distance: 1.54 Å) bonded to an oxygen atom in the resorcinol ring. Leucine 48 formed another HB (distance: 2.46 Å) with a hydrogen atom attached to the second oxygen in the resorcinol ring. HBs were also observed in lysine 112 (distance: 6.17 Å) and glycine 97 (length: 2.39 Å). Methionine 98 formed a π-sulphur interaction (distance: 5.46 Å) with a benzene ring. The isopropyl group formed an alkyl

interaction with valine 150 (distance: 4.52 Å), phenylalanine 138 (distance: 5.00 Å), and leucine 107 (distance: 5.09 Å). Other interactions on NVP with residues in the ATP binding site are vdW interactions.

Applying the rule of five

The Lipinski rule provides an approach for selecting compounds to be considered as drug candidates. Table 1 shows the conceptual properties considered when selecting molecules with good absorption or permeation. The compounds listed in the table all met Lipinski's rule of five, of which we selected the three bests for further investigation.

- Molecular weight (MW) $\leq$ 500.
- Calculated partition coefficient (cLog P) $\leq$ 5.
- The number of rotatable bonds (NRB) $\leq$ 10.
- The number of hydrogen bond donors (NHBD) $\leq$ 5.
- The number of hydrogen bond acceptors (NHBA) $\leq$ 9.

The interaction of hit compounds with the binding site

The hit compounds obtained by the virtual screening method showed that they interact with the ATP-binding site at the N-terminus of Hsp90 (Fig. S3). In the interactions of ZINC20411962 (A) in Figure S3A, threonine 184 HB showed 1.92 Å from the hydrogen atom bound to the nitrogen in the isoxazole ring. Aspartate 93 (distance: 1.62 Å) and leucine 48 (length: 2.45 Å) formed HBs with hydrogen atoms attached to the oxygen atoms of the resorcinol ring. Methionine 98 showed π-sulphur interactions with the isoxazole ring (distance: 4.03 Å) and a single benzene ring fragment linked to the carbonyl group (length: 5.34 Å). Other interactions of A are vdW-, alkyl- and π-alkyl-like. ZINC13120102, B (Figure S3B) formed an HB between a hydrogen atom attached to an oxygen atom on a resorcinol ring (distance: 3.09 Å) and glycine 135. Another HB appears between an oxygen atom in the resorcinol ring (length: 2.27 Å) and phenylalanine 138. The rest of the residues showed vdW, alkyl, and π-alkyl interactions. ZINC15905860 (Figure S3C) formed a hydrogen bond with glycine 137 across oxygen (distance: 3.05 Å) and nitrogen (distance: 3.16 Å) in the fused phenyl ring. Glycine 137 also shows a characteristic amide-π interaction with two different nitrogen atoms within the fused phenyl ring. Asparagine 51 formed hydrogen bonds with nitrogen (distance: 3.22 Å) on the fused phenyl ring, nitrogen (distance: 3.03 Å) in the amide group, and oxygen (distance: 3.28 Å) in its five-membered unit.

MD simulations

System stability

Molecular docking alone is not sufficient to provide accurate results on the interaction between enzymes and ligands [37]. Therefore, it is important to refine the docking results with MD simulations to gain better insight into the interactions of the Hit compounds in complex with the N-terminal Hsp90. The three Hit compounds with high binding affinity were subjected to 50-ns simulation to investigate their stability within the ATP pocket of the N-terminus of Hsp90. We use the metrics RMSD, RMSF, RoG and principal component analysis (PCA) to investigate the stability of the protein-ligand complex.

If we use the RMSD (Fig. 2A) of the free Hsp90 N-terminal enzyme (NT-apo) as a reference, we find a significant instability around 40 ns. The RMSD of all hit compounds was more stable than the RMSD of NT-apo, with ZINC20411962 being the most stable and ZINC13120102 even more stable. The hits thus showed relative stability within the active site throughout the simulation. The RMSF indicates the flexibility of the protein on a per-residue basis. The RMSF of the hit compounds (Fig. 2B) showed a slightly lower fluctuation of residues than the NT-apo. This result shows that the binding of the selected hits in the ATP pocket is stable, with ZINC20411962 being the most stable compound.

The compactness of the systems measured with RoG (Fig. 2C) provides information about the complex fluctuations of a rigid body. The ligand-protein complexes showed smaller RoG values compared to the NT-apo complex, indicating that the ligand-protein complexes are densely packed. The RoG values of the ZINC20411962 and ZINC13120102 complexes are lower than those of the other systems, indicating greater compactness of these systems. In addition, all systems showed stability, indicating that the hits obtained bind to the Hsp90 to an appreciable extent.

Fig. S4 shows the PCA plot for ZINC15905860, ZINC13120102, and ZINC20411962 along the direction of two principal components. ZINC15905860 occupies a larger phase-space and has a higher fluctuation, followed by ZINC13120102. ZINC20411962 shows less movement than the other two systems and appears to be the most stable with optimal affinity. The relative aggregation of ZINC20411962 PCA along its two vectors compared to the other systems is also consistent with the RMSD, RMSF, and RoG analyses.

Per-residue energy decomposition (PRED) analyses

We calculated the energy contribution of each residue to ligand binding using MMPBSA to gain deeper insight into each interaction. Fig. S5 shows the PRED (ΔE_{elec}, $\Delta E_{vdW,}$ and $\Delta E_{non\text{-}polar}$) profile showing the crucial residues involved in the binding of ZINC20411962, ZINC13120102, and ZINC15905860 to the ATP pocket of the Hsp90 N-domain. For ZINC20411962, leucine 48, aspartic acid 93 and threonine 184 ΔEelec show a favourable contribution to the total energy per residue. This supports the hydrogen bonding observed in Fig. S3A for these residues and the compound. Although lysine 58 also shows a high ΔE_{elec} contribution, we observe an unfavourable polar ΔE_{non} contribution, resulting in a very small ΔE_{total} and a

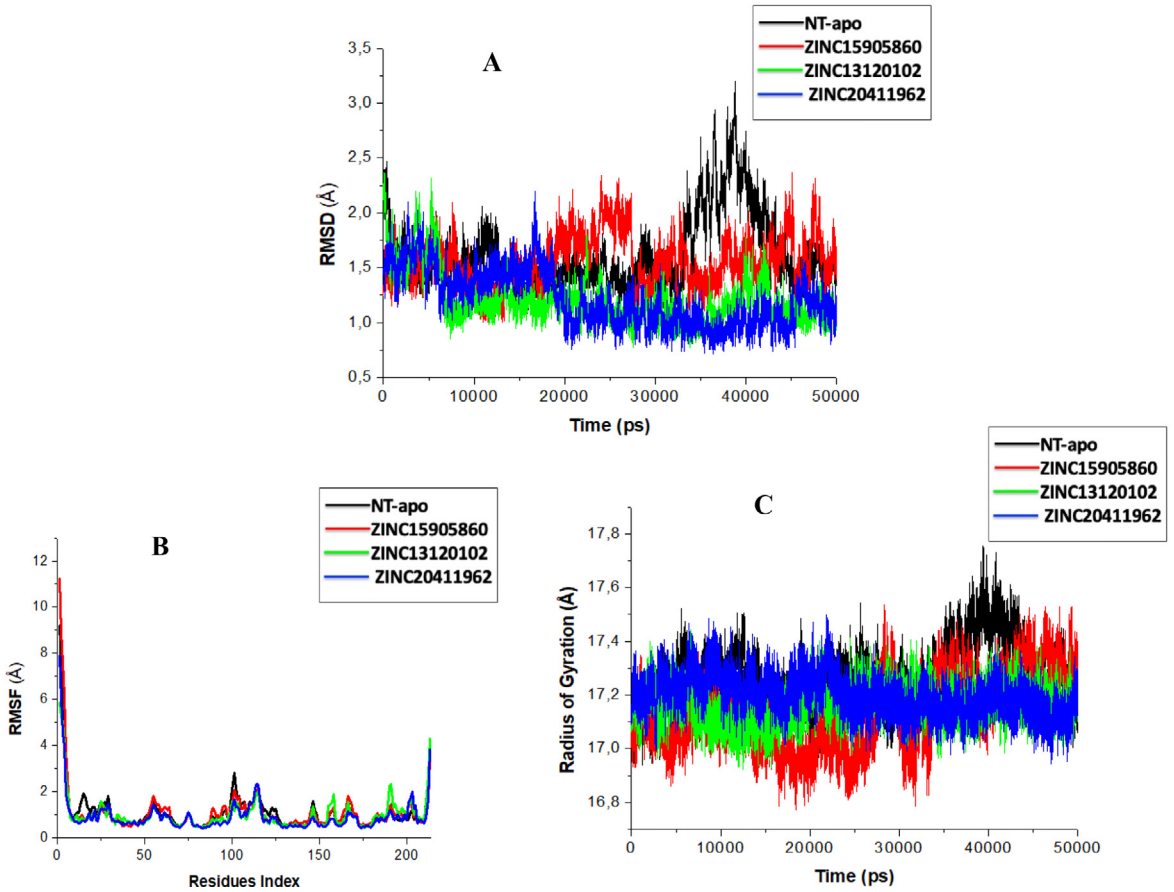

Fig. 2. The RMSD (A), RMSF (B), and RoG (C) plots for Hsp90 NT-apo, with Hsp90 NT complex of ZINC15905860, ZINC13120102, and ZINC20411962 recorded at 50 ns simulations.

negligible contribution from the residue. Asparagine 51 shows a significant ΔE_{vdW} affecting the ΔEtotal for this residue, which is consistent with the plot in Fig. S3A showing two carbon HB interactions between ZINC20411962 and this residue. Methionine 98 also shows a significant ΔEvdw contribution in all compounds, which is influenced by the π-sulphur and π-alkyl contributions observed in Fig. S3.

The energy distribution of ZINC13120102 (Fig. S5B) shows that asparagine 51 has favourable ΔE_{elec} and ΔE_{vdw} contributions, but unfavourable $\Delta E_{non\text{-}polar}$. Fig. S5B shows a favourable vdW interaction for asparagine 51, which could mean that $\Delta E_{non\text{-}polar}$ has an insignificant influence on the ΔEelec contribution. Moreover, the ΔEvdW interaction significantly affects the Δtotal sum between ZINC13120102 and its interfacial residues (Figs. S3B and S5B). Asparagine 51 also shows a high contribution (Fig. S5C) of ΔE_{vdW} and ΔE_{elec}, which is due to the three hydrogen bonds formed between this residue and ZINC15905860 (Fig. S3C). Alanine 55 shows ΔE_{vdW} contributions due to carbon HB interactions between this residue and the ligand (Fig. S3C)

Hydrogen bond network

HBs are special and play a central role in biological systems and in maintaining the structural integrity of proteins [38], protein-ligand interaction, and catalysis [38–40]. To further investigate the effects of the binding of the hit residues to the N-terminus of Hsp90, we estimate the evolution of hydrogen-bonding distances and the ratio between amino acid residues interacting with ZINC20411962, ZINC13120102, and ZINC15905860 in the active site for 50-ns simulations (Table S1). The residues that form the HBs are Asp93, Thr184, Leu48, Asn51, Lys58, Gly135, Asn106, and Phe138. Asp93, Thr184, and Asn106 are important binding sites of the N-terminus of Hsp90.

Table S1 shows that ZINC20411962 has hydrogen interactions with Asp93, Thr184, Leu48, and Lys58 with percentages of 99.9, 75.5, 36.9, and 14.6%, respectively. This estimate is consistent with PRED in Fig. S5A, with Asp93 showing a greater ΔE_{elec}, followed by Lys58. Lys58 shows a very high ΔE_{elec}, which is suppressed by ΔEnon-polar, reducing the ΔEelec influence. Therefore, Thr184 is a second ΔE_{elec} influenced residue, followed by Leu48 and then Lys58. ZINC13120102 shows HBs through Asn51, Thr152, and Gly135 with proportions of 12.5, 11.9, and 11.2%, respectively. This observation supports the

Table 2
Thermochemistry parameters (in kcal/mol) for potent inhibitor binding to Hsp90 N-terminal using B3LYP/6–31+G(d):AMBER QM/MM method.

	ΔE	ΔH	TΔS	ΔG_{bind}
ZINC15905860	–90.542	–79.729	–23.874	–55.855
ZINC13120102	–92.071	–85.895	–25.921	–59.974
ZINC20411962	–94.003	–91.079	–28.034	–63.045
NVP-AUY922 [23]	––	––	––	–49.400

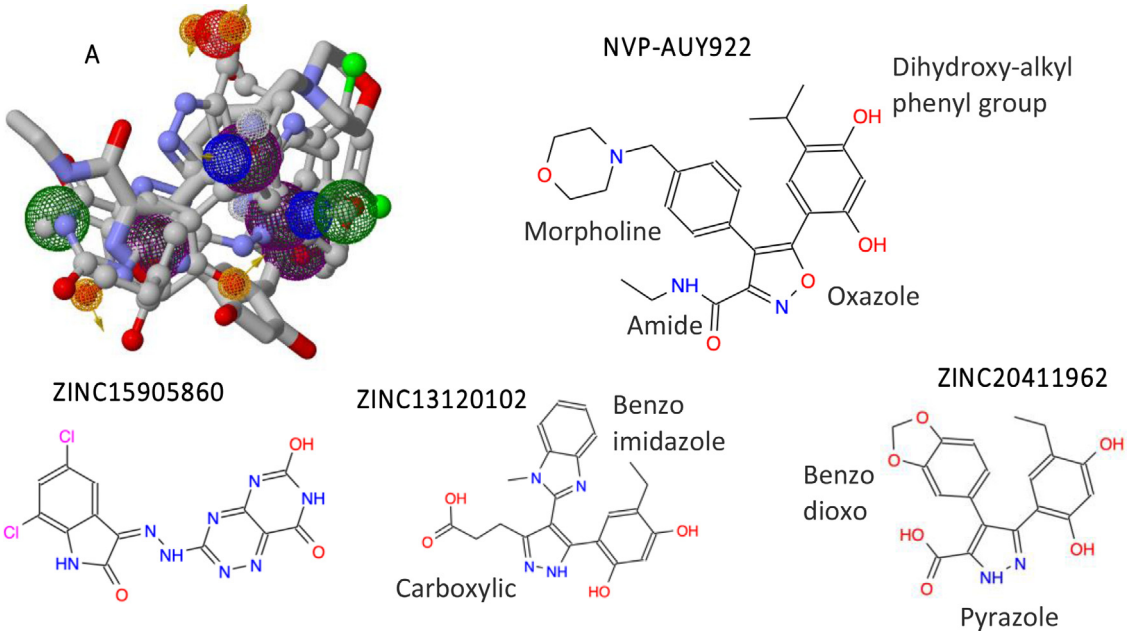

Fig. 3. The crucial mediators of NVP-AUY922, ZINC15905860, ZINC13120102, and ZINC20411962 necessary for optimum binding at the Hsp90 active site with their respective 2D structures indicating vital functional groups. In (A), purple = aromatic, white = hydrogen donor, yellow = hydrogen acceptor, blue = positive ion, red = negative ion, and green = hydrophobic.

PRED in Fig. S5B that Asn51 has a larger ΔE_{elec} driving the hydrogen interaction. ZINC15905860 shows hydrogen interactions with Phe138, Asn51, and Asn106 with proportions of 20.5, 3.6, and 1.8%, respectively.

Thermochemistry of the potent ligands binding to the Hsp90 using the ONIOM2 QM/MM approach

We examine the interaction of each potent ligand with the N-terminus of Hsp90 using the ONIOM model at the B3LYP/6–31+G(d) level of theory: AMBER, with residues Asn51, Ala55, Ile96, Met98, Asn106, Leu107, Val136, Phe138, Thr184 and the ligand at high levels. Table 2 shows that the total interaction energy (ΔE) and binding free energy (ΔG_{bind}) have favourable values; the more negative, the better the reactivity. Recall that a ΔG_{bind} value of Hsp90 N-terminal binding with NVP (the selected template) was observed to be –49.400 kcal/mol [23]. The ΔG_{bind} values for the potent inhibitors of Hsp90 N-terminal identified *in silico* are more favourable than NVP.

The enthalpy change (ΔH) is a representation of the energy transfer within a system [41]. The calculated negative ΔH values in Table 2 reflect an exergonic process for the interaction of these potent ligands with the N-terminus of Hsp90. The temperature-dependant entropy function (TΔS) could provide a basis for system stability, with a negative value indicating increasing order [42]. The order of the N-terminal Hsp90 complex with the selected ligands follows the trend ZINC15905860 < ZINC13120102 < ZINC20411962. The result implies that the last compound is the most stable during the binding process, as shown by the post-MD simulation metric.

Crucial moieties of the identified molecules and ADME study

Fig. 3 shows the functional groups controlling the binding of NVP-AUY922, ZINC15905860, ZINC13120102, and ZINC20411962 to the catalytic ATP pocket of Hsp90. NVP-AUY922, ZINC13120102, and ZINC20411962 are structurally related – they all have a 2,4-dihydroxyalkylphenyl moiety that enables hydrogen bonding with the polar and hydrophobic residues Leu48, Asp93, and Thr184 (Figs. S2 and S3). Other important scaffolds of NVP-AUY92 that enable inhibitory potential [22] are

Table 3
SwissADME [32] evaluation for ZINC15905860 (**A**), ZINC13120102 (**B**), and ZINC20411962 (**C**) showing indices from various theoretical framework.

	A	B	C		A	B	C
	Lipophilicity				Water Solubility		
Log $P_{o/w}$ (iLOGP)	1.27	1.98	1.62	Log *S* (ESOL)	−3.39	−4.31	−4.38
Log $P_{o/w}$ (XLOGP3)	1.25	2.94	3.26	Solubility	1.61e^{-1} mg/ml; 4.09e^{-4} mol/l	1.99e^{-2} mg/ml; 4.90e^{-5} mol/l	1.54e^{-2} mg/ml; 4.17e^{-5} mol/l
Log $P_{o/w}$ (WLOGP)	0.13	3.62	3.14	Class	Soluble	Moderately soluble	Moderately soluble
Log $P_{o/w}$ (MLOGP)	1.34	1.90	1.38	Log *S* (Ali)	−4.17	−5.21	−5.56
Log $P_{o/w}$ (SILICOS-IT)	1.69	3.61	3.24	Solubility	2.66e^{-2} mg/ml; 6.77e^{-5} mol/l	2.50e^{-3} mg/ml; 6.14e^{-6} mol/l	1.02e^{-3} mg/ml; 2.77e^{-6} mol/l
Consensus Log $P_{o/w}$	1.14	2.81	2.53	Class	Moderately soluble	Moderately soluble	Moderately soluble
Pharmacokinetics				Log *S* (SILICOS-IT)	−5.80	−6.09	−4.99
Gastrointestinal, GI absorption	Low	High	High	Solubility	6.27e^{-4} mg/ml; 1.60e^{-6} mol/l	3.33e^{-4} mg/ml; 8.18e^{-7} mol/l	3.80e^{-3} mg/ml; 1.03e^{-5} mol/l
CYP1A2 inhibitor	No	Yes	Yes	Class	Moderately soluble	Poorly soluble	Moderately soluble
Log K_p (skin permeation)	−7.81 cm/s	−6.69 cm/s	−6.23 cm/s				
Medicinal Chemistry	Drug likeness						
PAINS (Pan Assay Interference Structure)	1 alert: imine_one_isatin	0 alert	0 alert	Lipinski	Yes; 1 violation: N or *O* >10	Yes	Yes
Brenk	1 alert: imine_1	0 alert	0 alert	Ghose	Yes	Yes	Yes
Synthetic accessibility 1 (very easy) to 10 (very difficult)	2.97	3.34	3.24	Veber	No; 1 violation: TPSA>140	Yes	Yes
				Egan	No; 1 violation: TPSA>131.6	Yes	Yes
				Muegge	No; 1 violation: TPSA>150	Yes	Yes
				Bioavailability Score	0.55	0.56	0.56

N = nitrogen, *O* = oxygen, and TPSA = topological polar surface area.

methylated phenyl linked to morpholine, oxazole, and carboxamide. These functional units allow the identification of several compounds, including the selected ZINC15905860, ZINC13120102, and ZINC20411962. Only ZINC15905860 has a halogen functional unit (chlorine atoms) with eight different nitrogen networks and imine units. ZINC13120102 and ZINC20411962 have pyrazole units like the oxazole of NVP, with the benzo[d]imidazol-2-yl and the benzo[d][1,3]dioxol-6-yl of the respective compound corresponding to the 4-(morpholin-4-ylmethyl)phenyl fragment in NVP. All these functional groups exhibit pharmacophoric properties (Fig. 3A) that induce a molecular interaction at the catalytic site of the N-terminus of Hsp90. The pharmacophoric class is aromatic (benzene moiety), hydrogen donor (amine moiety), hydrogen acceptor (hydroxyl and carboxyl groups), positive ion (amine moiety), negative ion (carbonyl group), and hydrophobic (ether R-O-R).

To further predict the suitability of these compounds as plausible Hsp90 inhibitors, we estimate the ADME and pharmacokinetic properties to ensure the outcome is not a bias of one theory (Lipinski rule of 5). Our evaluation (Table 3) shows ZINC13120102 and ZINC20411962 as feasible compounds of interest while ZINC15905860 has poor outcomes. Fig. 3 also depicts the physicochemical properties of these compounds with mass (in g/mol) 393.14, 406.43, and 368.34 for ZINC15905860, ZINC13120102, and ZINC20411962, respectively. The ADME properties provided in Table 3 show that ZINC13120102 and ZINC20411962 are potential biomolecules that might inhibit the N-terminal of Hsp90 substantially. These compounds show appreciable lipophilicity index, gastrointestinal (GI) absorption, moderate solubility in water with favourable medicinal chemistry properties. They also align with all the drug-likeness theories with significant skin permeation and bioavailability scores.

Discussion

Researchers have applied CADD methods to find potent Hsp90 inhibitors with commendable results [9,10]. In this study, we use multidimensional in silico methods to identify plausible Hsp90 inhibitors based on an experimentally developed compound (NVP-AUY922 or NVP) reported to be at the clinical trial stage [22]. We identified novel N-terminal Hsp90 inhibitors by a virtual screening approach with binding propensity at the ATP pocket. Of the 77 molecules extracted from the database ZINC, the first three compounds with improved physicochemical properties and favourable binding energies compared to NVP-AUY922 have been selected.

The selected candidates for further investigation are ZINC20411962, ZINC13120102, and ZINC15905860. Interestingly, ganetespib (ZINC43130413) stood out in the screening procedure with a binding value of –8.7 kcal/mol, which is the same as that of ZINC15905860 and the lowest in our selection (Table 1). Ganetespib has been reported to significantly inhibit Hsp90 and has already been tested in many clinical trials [34] and human studies 49 [36]. This observation is thus an indication that the compounds obtained are likely to be potential anticancer drugs. Non-bonded interactions, including hydrogen bonds, π-alkyl, π-sulphur, and van der Waals, determine the binding process (Fig. S3). Docking results showed that ZINC20411962 performed better than the other two compounds and NVP itself with a binding affinity of –8.7 kcal/mol (Table 1). This value is more favourable than NVP with a value of –7.7 kcal/mol. We recall that an IC_{50} value of 0.1 μM was found in the literature for the inhibition of Hsp90 by NVP. Based on our CADD modelling, it is likely that ZINC20411962 could inhibit ten times better than NVP.

The RMSD, RMSF, RoG (Fig. 2), and PCA (Fig. S4) showed that these compounds were stable in the ATP pocket, with ZINC20411962 being the most stable compound. All three compounds interacted with the catalytic residues Thr184, Phe138, Met98 Gly97, and Asn106, which are critical for the inhibition of Hsp90 [9,10]. The decomposition of the energy per residue (Fig. S5) showed that the electrostatic and vdW contributions of the active residue significantly affected the total energy contribution. Hydrogen bonding profiling showed (Table S1) a significant contribution of the HBs to the structural stability of each complex.

Binding free energy calculation and thermodynamics of each system showed the suitability of these practically studied structures as potentially active inhibitors of the Hsp90 N domain (Table 2). The ONIOM calculation revealed very high energetic values for the binding of these potent molecules to the active pocket of the Hsp90 N domain, including the most reactive residues. Just like other simulations in this study, ZINC20411962 binds most stably and efficiently to the N-terminus of Hsp90 with an entropy value of –28 kcal/mol and a binding free energy value of –63 kcal/mol. Similarly, ZINC13120102 shows a remarkable binding affinity of about –60 kcal/mol. The ADME metrics suggest that ZINC20411962 and ZINC13120102 are likely inhibitors of Hsp90 NT with reasonable results (Table 3).

Conclusion

The alarming growth rate of cancer in humans requires durable therapeutic interventions where structure-based drug design is applicable. Using CADD modelling, we have identified three potentially active inhibitors of Hsp90 that bind to the ATP pocket. Further refinement of the identified molecules in complex with the Hsp90 model using different computational and theoretical approaches has shown that they are potentially active agents against their target. We started the study by building a pharmacophore model based on a known bioactive compound (NVP) that can significantly inhibit Hsp90 and is in clinical trials. Docking results show that more than 10 of the NVP-based ligands studied have better binding affinity than NVP itself. We then apply MD and QM/MM simulation studies to investigate three of these ten hit compounds with high binding results.

The crucial residues required for ATP binding to the active site of the N-terminus of Hsp90 also appear at the binding interfaces of the receptor for these new compounds, indicating their selectivity. All conceptual components investigated in this work support ZINC20411962 as a potential inhibitor of the N-domain of Hsp90. The MD simulation and QM/MM facilitate the investigation of the stability of the protein-ligand complex and the accurate estimation of the interaction energy. The pharmacokinetics, drug-like, ADME, and toxicity indices (medicinal chemistry) also favours this compound. Future research will involve the evaluation of ZINC20411962 as a drug candidate against cancer using an experimental protocol. If successful, this investigation will make an important contribution to anticancer drug design and could potentially serve as a lead molecule for structure-based inhibitor development.

In summary, we have identified new Hsp90 N-terminal inhibitors through various computational experiments. The identified compounds, including ZINC20411962 and ZINC13120102, have improved properties than the parent material NVP. Our screening also shows ZINC43130413 (ganetespib) – an ongoing clinical trial Hsp90 inhibitor, thereby buttressing the accuracy of the search protocol. Therefore, the identified compounds, especially ZINC20411962, might likely inhibit not just the Hsp90 N-terminal but the entire Hsp90 protein. In this study, we have used a protocol that is reproducible and convenient for computational and theoretical chemists, drug designers, biochemists, medicinal chemists, plus, synthetic chemists. The outcome will benefit pharmaceutical personnel, particularly those interested in cancer drug development. The compounds featured herein could be a starting point for the improved design of drugs against cancers of cervical, colon, liver, brain, kidney, lung, breast, and prostate. Besides, curbing and finding lasting solutions to all cancer types will ease the inherent burden on humans and the death rate associated with cancer in Africa. Therefore, a highly potent drug molecule will potentially reduce the cost of care and facilities required for cancer treatment/management, it will also slow down the expanding cancer mortality rates in Africa [43] and the world at large.

The outcome of this study would contribute to the African Union's Agenda 2063 on better health for all. The obtained compounds have propensities to inhibit Hsp90, representing a potential anticancer and paving the way for further hit compounds identification. Our methodology can also be adapted to identify phytocompounds of bio-importance from traditional African plants as Hsp90 inhibitors and anticancer candidates. The unique context of this research would encourage scientists to further apply and test existing medical theories and develop new theories to help stakeholders understand the African health business environment. Our investigation has addressed the "progress and collective prosperity" goal of the African Union's Agenda 2063 by suggesting a solution to a pertinent issue ravaging our race. A sustainable solution to cancer will preserve the African race to have more persons of intellect that would drive the 2063 Agenda of making Africa the powerhouse of the world.

Declaration of Competing Interest

The authors declare no conflict of interest.

Acknowledgements

We acknowledge the College of Health Sciences, University of KwaZulu-Natal, Durban, South Africa, South African National Research Foundation for supporting this study, and the Centre for High-Performance Computing, South Africa (www.chpc.ac.za) for the computational resource.

Supplementary materials

Supplementary material associated with this article can be found, in the online version, at doi:10.1016/j.sciaf.2022.e01107.

References

[1] J.C. Young, I. Moarefi, F.U. Hartl, Hsp90: a specialized but essential protein-folding tool, J. Cell Biol. 154 (2001) 267.
[2] S. Saxena, S.S. Chaudhaery, K. Varshney, A.K. Saxena, Pharmacophore-based virtual screening and docking studies on Hsp90 inhibitors, SAR QSAR Environ. Res. 21 (2010) 445–462.
[3] G. Crevel, H. Bates, H. Huikeshoven, S. Cotterill, The drosophila dpit47 protein is a nuclear Hsp90 co-chaperone that interacts with DNA polymerase α, J. Cell Sci. 114 (2001) 2015–2025.
[4] M. Ferrarini, S. Heltai, M.R. Zocchi, C. Rugarli, Unusual expression and localization of heat-shock proteins in human tumor cells, Int. J. Cancer 51 (1992) 613–619.
[5] A. Shimomura, N. Yamamoto, S. Kondo, Y. Fujiwara, S. Suzuki, N. Yanagitani, A. Horiike, S. Kitazono, F. Ohyanagi, T. Doi, First-in-human phase I study of an oral Hsp90 inhibitor, TAS-116, in patients with advanced solid tumors, Mol. Cancer Ther. 18 (2019) 531–540.
[6] O.M. Grbovic, A.D. Basso, A. Sawai, Q. Ye, P. Friedlander, D. Solit, N. Rosen, V600E B-Raf requires the Hsp90 chaperone for stability and is degraded in response to Hsp90 inhibitors, Proc. Natl. Acad. Sci. 103 (2006) 57–62.
[7] R. Roskoski, Anaplastic lymphoma kinase (ALK): structure, oncogenic activation, and pharmacological inhibition, Pharmacol. Res. 68 (2013) 68–94, doi:10.1016/j.phrs.2012.11.007.
[8] R.I. Nicholson, J.M.W. Gee, M.E. Harper, EGFR and cancer prognosis, Eur. J. Cancer. 37 (2001) 9–15, doi:10.1016/S0959-8049(01)00231-3.
[9] B. Birbo, E.E. Madu, C.O. Madu, A. Jain, Y. Lu, Role of HSP90 in Cancer, Int. J. Mol. Sci. 22 (2021) 10317.
[10] H.K. Park, N.G. Yoon, J.E. Lee, S. Hu, S. Yoon, S.Y. Kim, J.H. Hong, D. Nam, Y.C. Chae, J.B. Park, Unleashing the full potential of Hsp90 inhibitors as cancer therapeutics through simultaneous inactivation of Hsp90, Grp94, and TRAP1, Exp. Mol. Med. 52 (2020) 79–91.
[11] V.A. Johnson, E.K. Singh, L.A. Nazarova, L.D. Alexander, S.R. McAlpine, Macrocyclic inhibitors of Hsp90, Curr. Top. Med. Chem. 10 (2010) 1380–1402, doi:10.2174/156802610792232088.

[12] G. Chiosis, L. Neckers, Tumor selectivity of Hsp90 inhibitors: the explanation remains elusive, ACS Chem Biol 5 (2006) 279–284, doi:10.1021/cb600224w.
[13] A. Kamal, L. Thao, J. Sensintaffar, L. Zhang, M.F. Boehm, L.C. Fritz, F.J. Burrows, A high-affinity conformation of Hsp90 confers tumour selectivity on Hsp90 inhibitors, Nature 425 (2003) 407.
[14] L. Neckers, P. Workman, Hsp90 molecular chaperone inhibitors: are we there yet? Clin. Cancer Res. 18 (2012) 64–76.
[15] K. Jhaveri, T. Taldone, S. Modi, G. Chiosis, Advances in the clinical development of heat shock protein 90 (Hsp90) inhibitors in cancers, Biochim. Biophys. Acta (BBA) Mol. Cell Res. 1823 (2012) 742–755.
[16] R. Garcia-Carbonero, A. Carnero, L. Paz-Ares, Inhibition of Hsp90 molecular chaperones: moving into the clinic, Lancet Oncol. 14 (2013) e358–e369.
[17] A.K. Saxena, S. Saxena, S.S. Chaudhaery, Molecular modelling and docking studies on heat shock protein 90 (Hsp90) inhibitors, SAR QSAR Environ. Res. 21 (2010) 1–20.
[18] R. Sanam, S. Tajne, R. Gundla, S. Vadivelan, P.K. Machiraju, R. Dayam, L. Narasu, S. Jagarlapudi, N. Neamati, Combined pharmacophore and structure-guided studies to identify diverse Hsp90 inhibitors, J. Mol. Gr. Model. 28 (2010) 472–477.
[19] S. Sakkiah, S. Thangapandian, S. John, K.W. Lee, Pharmacophore based virtual screening, molecular docking studies to design potent heat shock protein 90 inhibitors, Eur. J. Med. Chem. 46 (2011) 2937–2947.
[20] S. Sakkiah, S. Thangapandian, S. John, Y.J. Kwon, K.W. Lee, 3D QSAR pharmacophore based virtual screening and molecular docking for identification of potential Hsp90 inhibitors, Eur. J. Med. Chem. 45 (2010) 2132–2140.
[21] R. Huang, D.M. Ayine-Tora, M.N.M. Rosdi, Y. Li, J. Reynisson, I.K.H. Leung, Virtual screening and biophysical studies lead to Hsp90 inhibitors, Bioorg. Med. Chem. Lett. 27 (2017) 277–281.
[22] A.D. Zuehlke, M.A. Moses, L. Neckers, Heat shock protein 90: its inhibition and function, Philos. Trans. R. Soc. B Biol. Sci. 373 (2018) 20160527, doi:10.1098/rstb.2016.0527.
[23] A.M. Magwenyane, N.N. Mhlongo, M.M. Lawal, D.G. Amoako, A.M. Somboro, S.C. Sosibo, L. Shunmugam, R.B. Khan, H.M. Kumalo, Understanding the Hsp90 N-terminal dynamics: structural and molecular insights into the therapeutic activities of anticancer inhibitors radicicol (RD) and radicicol derivative (NVP-YUA922), Molecules 25 (2020) 1785, doi:10.3390/molecules25081785.
[24] J. Liu, W. Sun, W. Dong, Z. Wang, Y. Qin, T. Zhang, H. Zhang, Hsp90 inhibitor NVP-AUY922 induces cell apoptosis by disruption of the survivin in papillary thyroid carcinoma cells, Biochem. Biophys. Res. Commun. 487 (2017) 313–319.
[25] C. Prodromou, S.M. Roe, R. O'Brien, J.E. Ladbury, P.W. Piper, L.H. Pearl, Identification and structural characterization of the ATP/ADP-binding site in the Hsp90 molecular chaperone, Cell 90 (1997) 65–75.
[26] E.F. Pettersen, T.D. Goddard, C.C. Huang, G.S. Couch, D.M. Greenblatt, E.C. Meng, T.E. Ferrin, UCSF chimera—a visualization system for exploratory research and analysis, J. Comput. Chem. 25 (2004) 1605–1612, doi:10.1002/jcc.20084.
[27] O. Trott, A.J. Olson, AutoDock Vina: improving the speed and accuracy of docking with a new scoring function, efficient optimization, and multithreading, J. Comput. Chem. 31 (2010) 455–461, doi:10.1002/jcc.21334.
[28] G.M. Morris, R. Huey, W. Lindstrom, M.F. Sanner, R.K. Belew, D.S. Goodsell, A.J. Olson, AutoDock4 and AutoDockTools4: automated docking with selective receptor flexibility, J. Comput. Chem. 30 (2009) 2785–2791, doi:10.1002/jcc.21256.
[29] T. Hou, J. Wang, Y. Li, W. Wang, Assessing the performance of the MM/PBSA and MM/GBSA methods. 1. The accuracy of binding free energy calculations based on molecular dynamics simulations, J. Chem. Inf. Model. 51 (2010) 69–82.
[30] L. Xu, H. Sun, Y. Li, J. Wang, T. Hou, Assessing the Performance of MM/PBSA and MM/GBSA Methods. 3. The Impact of force fields and ligand charge models, J. Phys. Chem. B. 117 (2013) 8408–8421, doi:10.1021/jp404160y.
[31] R.A. Copeland, M.R. Harpel, P.J. Tummino, Targeting enzyme inhibitors in drug discovery, Expert Opin. Ther. Targets 11 (2007) 967–978, doi:10.1517/14728222.11.7.967.
[32] A. Daina, V. Zoete, A boiled-egg to predict gastrointestinal absorption and brain penetration of small molecules, ChemMedChem 11 (2016) 1117.
[33] L. Pauling, L.O. Brockway, Carbon—carbon bond distances. The electron diffraction investigation of ethane, propane, isobutane, neopentane, cyclopropane, cyclopentane, cyclohexane, allene, ethylene, isobutene, tetramethylethylene, mesitylene, and hexamethylbenzene, Rev. Values J. Am. Chem. Soc. 59 (1937) 1223–1236.
[34] A. Yuno, M.J. Lee, S. Lee, Y. Tomita, D. Rekhtman, B. Moore, J.B. Trepel, in: Clinical Evaluation and Biomarker Profiling of Hsp90 Inhibitors, Springer, Chaperones, 2018, pp. 423–441.
[35] E.B. Garon, T. Moran, F. Barlesi, L. Gandhi, L.V. Sequist, S.W. Kim, H.J.M. Groen, B. Besse, E.F. Smit, D.W. Kim, M. Akimov, E. Avsar, S. Bailey, E. Felip, Phase II study of the Hsp90 inhibitor AUY922 in patients with previously treated, advanced non-small cell lung cancer (NSCLC), J. Clin. Oncol. 30 (2012) 7543, doi:10.1200/jco.2012.30.15_suppl.7543.
[36] I. Ray-Coquard, I. Braicu, R. Berger, S. Mahner, J. Seouli, E. Pujade-Lauraine, P.A. Cassier, U.M. Moll, H. Ulmer, K. Leunen, Part I of GANNET53: a European multicenter phase I/II trial of the Hsp90 inhibitor ganetespib combined with weekly paclitaxel in women with high-grade, platinum-resistant epithelial ovarian cancer–a study of the GANNET53 consortium, Front. Oncol. 9 (2019) 832.
[37] T. Pantsar, A. Poso, Binding affinity via docking: fact and fiction, Molecules 23 (2018) 1899, doi:10.3390/molecules23081899.
[38] G.A. Jeffrey, W. Saenger, Hydrogen Bonding in Biological Structures, Springer Berlin Heidelberg, Berlin, Heidelberg, 1991, doi:10.1007/978-3-642-85135-3.
[39] D. Hornby, Hydrogen bonding in biological structures, FEBS Lett. 323 (1993) 295 295, doi:10.1016/0014-5793(93)81362-4.
[40] S.J. Grabowski, Hydrogen Bonding—New Insights, Springer, Netherlands, 2006, doi:10.1007/978-1-4020-4853-1.
[41] A.D. Becke, Density-functional thermochemistry. II. The effect of the Perdew–Wang generalized-gradient correlation correction, J. Chem. Phys. 97 (1992) 9173–9177, doi:10.1063/1.463343.
[42] M.M. Lawal, T. Govender, G.E.M. Maguire, B. Honarparvar, H.G. Kruger, Mechanistic investigation of the uncatalyzed esterification reaction of acetic acid and acid halides with methanol: a DFT study, J. Mol. Model. 22 (2016) 235.
[43] Z. Chen, L. Xu, W. Shi, F. Zeng, R. Zhuo, X. Hao, P. Fan, Trends of female and male breast cancer incidence at the global, regional, and national levels, 1990–2017, Breast Cancer Res. Treat. 180 (2020) 481–490, doi:10.1007/s10549-020-05561-1.